

Simulation of the formation and detection of one-dimensional ordered ion beams

Joanne Beebe-Wang, Nils Elander, and Reinhold Schuch

Atomic Physics, Department of Physics, Stockholm University, Frescativägen 24, S-10405 Stockholm, Sweden

(Received 6 May 1994; revised manuscript received 25 July 1994)

Ion beam ordering in a realistic cooler storage ring was investigated using a molecular dynamics computer code developed for this study. A parameter $C(T)$ was introduced to quantify ordering effects in ion beams as a function of temperature. The code was applied to singly (Li^+) and highly (Ar^{18+}) charged ion beams under the action of longitudinal (laser) and uniform (electron) cooling in CRYRING (Stockholm storage ring). It was found that one-dimensional (1D) ordering can be formed in dilute ($\sim 10^6$ particles) Li^+ and Ar^{18+} beams at longitudinal temperatures ~ 1 and $\sim 10^2$ mK, respectively, even for relatively high transverse temperatures. The heat exchange between longitudinal and transverse degrees of freedom in singly and highly charged ion systems was compared under similar conditions. High-frequency longitudinal Schottky spectra are derived by fast Fourier transforms, to illustrate a possible method of observing 1D ordering of ion beams in storage rings.

PACS number(s): 41.75.-i, 29.20.Dh, 52.25.Wz, 52.65.+z

I. INTRODUCTION

A new generation of ion accelerators, i.e., cooler storage rings, has been developed in recent years. These machines provide acceleration and storage of ion beams and include electron, laser, or stochastic cooling to increase ion beam phase space densities [1]. As a consequence of cooling, the coupling between ions via the Coulomb force becomes significant, and collective modes in the beams become visible [2]. With the prospect of even lower ion temperatures, it has been proposed that the ions may arrange themselves in a crystalline structure as they circulate in a storage ring [3]. Crystallized ion beams in storage rings are of considerable interest. The crystals, with macroscopic size (~ 50 m) and densities of $10^4 - 10^7$ ions/cm³, would constitute the most dilute form of crystalline matter known with very different properties as compared with crystals of the solid state. Cooling a stored ion beam to a crystal state would eliminate intrabeam scattering and decrease the velocity spread, thereby decreasing the Doppler widths of absorption and emission lines observed in spectroscopy experiments. It could also be possible to enhance luminosities in future colliders by using crystallized beams, so that the particles would not collide in a random fashion, but in an ordered way. The possibility to investigate this form of matter and to study ordering transitions has recently drawn great interest and much activity [4].

An early observation of crystallization and melting of a trapped charged particle system was reported [5] in 1959. In recent years, several experimental investigations of ordering of singly charged ions, such as Mg^+ , Hg^+ , and Ba^+ , in Paul traps [6] and Penning traps [7] by laser cooling have been carried out. In 1992, Waki *et al.* successfully crystallized Mg^+ ion systems in a ring shaped rf quadrupole trap with laser cooling and obtained concentric cylindrical shell structures [8].

The only experimental evidence on crystallization of

charged particle beams in a synchrotron storage ring was obtained in NAP-M at Novosibirsk in 1980 [9]. During cooling of a proton beam the random noise in the Schottky pickup detector decreased to a low and constant value. Later, this observation was interpreted as a transition from a random to an ordered phase in a strongly coupled one-component plasma (OCP) [10] and became the starting point of a series of investigations concerning beam crystallization in storage rings. The first study of ion beam crystallization by molecular dynamics (MD) simulation was reported by Rahman and Schiffer in 1986 [11]. A stationary plasma was simulated in a constant cylindrically symmetric harmonic potential. At low temperatures, the particles populated concentric cylindrical shells around the beam axis and formed a hexagonal lattice on the mantle of each shell. It was also stated that investigations on shear and periodic focusing forces were needed before one could predict whether this form of ordering would be possible to achieve in a real storage ring. In some later works, the structure and the excess energy of cylindrical Coulomb crystal in the same idealized model were studied in more details [12–15] and, by adding shear velocity and periodically turning on and off a focusing force, the beam radius and temperature were investigated [12,16]. Hofmann *et al.* [17] discussed the theoretical maximum cooling rate and its interplay with heating by intrabeam scattering and collective instabilities in realistic storage ring lattices. Realistic simulations of ion beam crystallization in an existing cooler storage ring using molecular dynamics were carried out by the current authors [18]. Recently, Wei *et al.* investigated the ground state and critical temperatures for crystalline beams in realistic storage ring lattices [19].

In the present work, we simulate the formation and storage of one-dimensional (1D) ordered ion beams in a realistic cooler storage ring lattice. The method of modeling circulating ions in a storage ring using molecular dynamics is presented in Sec. II. The treatment of the

external fields is described in Sec. II A; the method of handling the interparticle forces of a large number of ions is described in Sec. II B; modeling of the cooling process is described in Sec. II C; and a measure of the ordering of the ion system is introduced in Sec. II D. The application of the method to an existing storage ring—CRYRING—is presented in Sec. III. The lattice values of the storage ring were reproduced with our MD calculations, demonstrating that the beam optics of the ring were correctly included. The simulation results of singly (Li^+) and highly (Ar^{18+}) charged ion beams under the action of longitudinal (laser) and uniform (electron) cooling are presented in Sec. IV. In Sec. V, Schottky noise analysis is discussed as a possible detection scheme for 1D ordered structures. Conclusions and discussions of the results are given in Sec. VI.

II. MODELING OF THE ION MOTION IN A STORAGE RING

For a classical system of N identical ions of mass m and charge q in the fields of a storage ring, the equation of motion of the i th ion can be written as

$$m \frac{d^2 \mathbf{r}_i}{dt^2} = q \mathbf{v}_i \times \mathbf{B}^{\text{ext}}(\mathbf{r}_i) + \sum_{j \neq i}^N \frac{q^2 (\mathbf{r}_i - \mathbf{r}_j)}{4\pi \epsilon_0 r_{ij}^3}, \quad (1)$$

where \mathbf{r}_i and \mathbf{v}_i are the position and velocity of the i th ion, $\mathbf{B}^{\text{ext}}(\mathbf{r}_i)$ is the external magnetic field in the storage ring, and ϵ_0 is the dielectric constant. Here we are treating the situation of a coasting beam, i.e., without acceleration. The laboratory velocities of the ions in most of storage rings are in the range of $\beta = \frac{v_0}{c} \sim 10^{-2} - 10^{-1}$. Thus it is unnecessary to take relativistic effects into account. Since the distances between the ions range from 10 μm to more than 100 μm , we can treat the system as purely classical. Further, we neglect the effect of image charges in the vacuum containment induced by the ions.

In this work, two coordinate systems are used: the external fields in the storage ring are described by a coordinate system (X, Y, s) in the laboratory frame; the ion motions are observed in the frame moving with beam velocity \mathbf{v}_0 using the coordinate system (x, y, z) . The coordinates (X, Y, s) are defined as follows: The X and Y axes lay in the plane perpendicular to the beam direction with the X axis in the dispersion plane of the dipole magnets and Y axis perpendicular to it. The s coordinate is the distance measured along the central orbit in the beam direction with the beginning of the first superperiod defined as $s = 0$. The coordinates (x, y, z) are defined as $x \parallel X$, $y \parallel Y$ and z axes in the beam direction with the origin placed in the center of the beam at the beginning of the basic cell (see Sec. II B).

The equation of motion is solved with the molecular dynamics method [20,21] by expressing the position of each particle at a time $t + \delta t$ in terms of the two previous positions at t and $t - \delta t$ and the accelerations at time t . The time step δt should be small enough to allow the approximation of a linear motion during δt .

A. Treatment of the external fields

1. Focusing-defocusing effects

The focusing-defocusing effects are mainly coming from the quadrupole magnets and the fringe fields of the bending magnets. With its hyperbolic shaped poles, a normal quadrupole magnet provides the magnetic field $\mathbf{B}_q = G(Y\hat{\mathbf{e}}_X + X\hat{\mathbf{e}}_Y)$, where G is the field gradient and $\hat{\mathbf{e}}_X, \hat{\mathbf{e}}_Y$ are unit vectors in the X and Y directions. An ion with velocity \mathbf{v}_0 is subject to a Lorentz force $\mathbf{F}_q = qv_0 G(-X\hat{\mathbf{e}}_X + Y\hat{\mathbf{e}}_Y)$, restoring in one direction and repelling in the other. The components in both directions are linear with the displacements. The ends of bending magnets may also have focusing-defocusing effects on a beam, with the strength and the focal plane dependent on the particular design. These effects can also be expressed in the same linear form. As a result, we can express the focusing-defocusing effects in the ring through a force containing quadrupole strengths $k_X(s)$ and $k_Y(s)$:

$$\mathbf{F} = k_X(s)X\hat{\mathbf{e}}_X + k_Y(s)Y\hat{\mathbf{e}}_Y. \quad (2)$$

Here $k_u(s) > 0$ causes focusing and $k_u(s) < 0$ causes defocusing in the u direction ($u = X, Y$) at ring location s . As the zeroth order approximation, a step function $k_u(s)$ can be constructed by the normalized quadrupole strengths of all the N_u contributing elements. For a more accurate simulation, we express $k_u(s)$ with a smoothly varying function to include the edge effects of the magnets:

$$k_u(s) = \sum_{n_u}^{N_u} K_{n_u}^u \left[\arctan \left(\frac{\pi}{C_{n_u}} (s - S_{n_u}^b) \right) + \arctan \left(\frac{\pi}{C_{n_u}} (S_{n_u}^e - s) \right) \right], \quad (3)$$

where $S_{n_u}^b$ and $S_{n_u}^e$ are the s coordinates at which the n_u th element begins and ends, respectively. $K_{n_u}^u$ is the normalized quadrupole strength at the center of the n_u th element. C_{n_u} is an adjustable parameter that gives a measure of the edge effect of the n_u th element and can be chosen to fit the field measurement.

2. Bending effects

When an ion traverses the bending magnet field $\mathbf{B}_m = -B_m \hat{\mathbf{e}}_Y$ with velocity $\mathbf{v}_i = \mathbf{v}_0 + \mathbf{w}_i$, there are shear effects (caused by $\mathbf{v}_0 \times \mathbf{B}_m$ and finite beam size) and higher order effects (caused by $\mathbf{w}_i \times \mathbf{B}_m$). The shear effect in a bending magnet is illustrated in Fig. 1. Consider two ions moving parallel to each other before entering a bending magnet. In the beam coordinates (x, y, z) , parallel means $z_1 = z_2 = 0$. Assume that ion No. 1 enters the magnet at point O on the central orbit ($x_1 = 0$) and ion No. 2 enters the magnet at point P on an outer orbit ($x_2 < 0$). After traversing the same distance δs in the bending magnet, ion No. 2 moves to P' while ion No. 1, which is at the

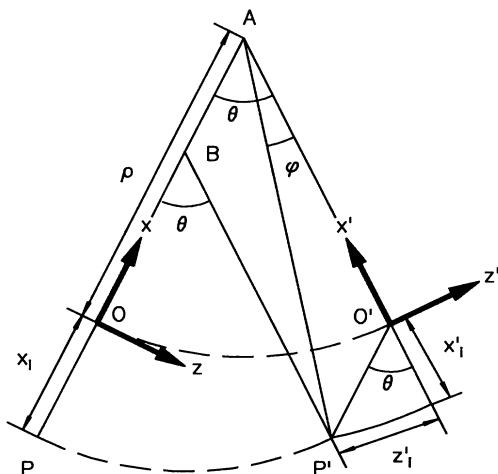


FIG. 1. The shear effect: Consider two ions at positions $z_1 = z_2 = 0$ before entering a bending magnet (z is coordinated in the beam direction). After traversing the same distance in the bending magnet, ion No. 2 moving from P to P' on an outer orbit is behind ion No. 1, which moves with the origin of the coordinates on the central orbit from O to O' . The two ions no longer have the same z coordinates ($z'_1 \neq z'_2$).

origin of the coordinates, moves to O' . With respect to the beam frame, ion No. 2 is behind ion No. 1, ($z'_1 = 0, z'_2 < 0$), so the two ions are no longer parallel to each other. This effect is called the “shear effect” and it may prevent the formation of crystals or cause distortions of crystal structures.

It can be easily seen, from Fig. 1, that the shear effect can be modeled by describing how the ion positions in the (x, y, z) coordinates are transformed to the (x', y', z') coordinates while the frame moves along with the beam. When the beam traverses a distance δs in a bending magnet, the original point of the beam frame translates from O to O' along a curved line s , which has a bending radius ρ and a rotating center A . Meanwhile, the orientation of the beam coordinates changes by an angle of $\theta = \frac{\delta s}{\rho}$. At the same time, an off-center ($x \neq 0$) ion moves from P to P' along a different curvature with the same radius ρ but around the rotating center B . Due to the nonzero x value, a change in the z value appears in the new coordinates (x', y', z') , which results in an additional angle φ with respect to the x' axis. Using the geometrical relation shown in Fig. 1, the shear effect can be described by a (x, z) transformation of the ion positions:

$$x' = (\rho^2 + 2\rho x \cos \theta + x^2)^{\frac{1}{2}} - \rho, \quad (4)$$

$$z' = z + (\rho^2 + 2\rho x \cos \theta + x^2)^{\frac{1}{2}} \varphi, \quad (5)$$

with

$$\varphi = \arctan \left(\frac{x \sin \theta}{\rho + x \cos \theta} \right). \quad (6)$$

If $\rho \gg x$ (as in most storage rings), Eqs. (4) and (5) can be reduced to

$$x' = x \cos \theta, \quad (7)$$

$$z' = z + x \sin \theta. \quad (8)$$

A higher order effect in the bending magnet is dispersion, which describes the closed orbit deviation of an ion with a slightly different momentum $m\mathbf{v}_i$ from the average ion momentum $m\mathbf{v}_0$. This effect is taken into account by including $\Delta\mathbf{F} = q\mathbf{w}_i \times \mathbf{B}_m$. The component $\Delta F_x = qB_m w_z$ is responsible for dispersion, whereas $\Delta F_z = -qB_m w_x$ contributes to chromaticity, which relates momentum spread to tune spread. Including this additional force in our MD simulations, the coupling of x and z motions caused by bending magnets is also incorporated.

3. Effects of solenoids and toroids

An electron cooler section consists of solenoids and toroids [22]. The main effect of a solenoidal field \mathbf{B}_s is to rotate the ions around the longitudinal axis with an angular frequency $\omega = \frac{qB_s}{m}$ [23]. In our simulation of crystallization by cooling with electrons, a rotation transformation of a small angle $\omega\delta t$ was performed at each time step δt inside the solenoids. The focusing effect of the solenoidal field and the effects of the magnetic field in a toroid are usually small and corrected immediately, so they do not need to be included in the simulations.

B. “Basic cell” model

The typical number of ions in a storage ring is $N = 10^5 - 10^9$. In the MD simulations, the computational effort grows linearly with N for the external forces, but grows as $N(N-1)/2$ for the interparticle Coulomb interactions. With currently available computers, it is impractical to perform MD simulations with all ions included. In such cases, the number of ions involved in the calculation can be reduced by introducing the “basic cell” and periodic boundary conditions. In our model, the ion beam is divided into N_c equal cells along the central orbit. Each cell has a diameter of the maximum beam size imposed by the acceptance of the storage ring and a length l . The Ewald [24] summation technique is generally used for summing the interactions between the ions in the basic cell and their periodic images. However, this technique was developed for ionic crystals in uniform backgrounds with homogeneous charge densities, and the summation is made in all dimensions. In a storage ring, the field varies over the typical length of Ewald summation, so does the charge distribution, and the summation should be made only along the ring. The Ewald summation technique is thus not directly applicable to the systems in a storage ring unless an appropriate correction is included. To incorporate such a modification, another order of magnitude of computer CPU time consumption

is required. Therefore, we resort to a practical solution by computing the interparticle interactions among the ions in the basic cell and the nearest neighboring cells, with a judicious choice of l to assure correct results.

The basic cell length l , on one hand, should be much shorter than the typical length over which the external fields vary so that the Hamiltonian is approximately invariant to translations over $\pm l$ in the beam direction. On the other hand, l should be long enough so that the crystalline structures are independent of the choice of l . It was concluded by a series of tests that, when l is large enough ($l \sim 1$ mm in most cases), the simulation results are dependent neither on the choice of l nor on the ions in more distant cells.

When an ion moves out of the basic cell radially, we consider it as being lost into the vacuum chamber. Since this occurs in each of the N_c cells equivalently, N_c ions are lost from the entire beam. On the other hand, when an ion moves out of the basic cell axially, it is replaced by another ion entering the basic cell from the opposite axial boundary with the same velocity; i.e., N_c ions have higher (or lower) momenta than the average value, but in this case no ions are lost from the beam.

This basic cell model retains the essential beam properties while largely reducing the computational effort needed to make the simulation practical. However, this model has certain limitations. First, it is not suitable to use the code to calculate tunes and dispersion functions by tracking a single particle in a longitudinally “hot” beam, because, if the ion momentum differs from the average, it will move out of the basic cell longitudinally and the tracking will be changed to a substitute particle. Second, this model does not include any effects with an active length longer than that of the basic cell l . For example, once a crystalline structure is formed in the beam, only oscillation modes with wavelengths λ_n , which satisfy $n\lambda_n = l$ (n is any positive integer), can survive. This applies also to the case where Schottky spectra should be derived; see Sec. V. In addition, one obtains a series of harmonics and their sidebands in the Schottky spectrum related to the beam velocity v_0 and cell length l .

C. Simulation of cooling effects

Ion beam cooling is a process which increases the phase space density of the ion beam. In a MD scheme, cooling is usually implemented by scaling the relative velocity, $\mathbf{w}_i = \mathbf{v}_i - \mathbf{v}_0$, of each ion at each time step δt by a factor f . To quantitatively describe the statistical behavior of the ion motion in different degrees of freedom, we associate the widths of the ion velocity distribution with a longitudinal temperature defined as

$$T_{\parallel} = \frac{m}{Nk_B} \sum_{i=1}^N w_{iz}^2 \text{ and a transverse temperature defined}$$

$$\text{as } T_{\perp} = \frac{m}{2Nk_B} \sum_{i=1}^N (w_{ix}^2 + w_{iy}^2).$$

With the notation $\zeta \equiv_{\parallel, \perp}$, the longitudinal and transverse cooling factors, in our model, are of the form

$$w'_{i\zeta} = f_{\zeta}(T_{\zeta}, T_{\zeta}^c, \gamma_{\zeta}) w_{i\zeta} = \left[1 - 2\gamma_{\zeta} \delta t \left(1 - \frac{T_{\zeta}^c}{T_{\zeta}} \right) \right]^{\frac{1}{2}} w_{i\zeta}, \quad (9)$$

where γ_{ζ} and T_{ζ}^c are the respective cooling strengths and the cooling medium temperatures. These cooling factors are characteristic of a system of particles that undergo frequent collisions with light particles of an ideal gas at fixed temperatures T_{\parallel}^c and T_{\perp}^c [25]. It can be shown that the cooling factors f_{\parallel} and f_{\perp} in the simulations are associated with the cooling forces F_{\parallel} and F_{\perp} , used to describe electron and laser cooling, through the relationship

$$f_{\zeta} = 1 + \frac{F_{\zeta}}{mw_{i\zeta}} \delta t. \quad (10)$$

The first order approximation to F_{ζ} is

$$F_{\zeta} \approx -\gamma_{\zeta} mw_{i\zeta} \left(1 - \frac{T_{\zeta}^c}{T_{\zeta}} \right). \quad (11)$$

Three cooling methods are now available for ion storage rings: electron cooling [22], laser cooling [26], and stochastic cooling [27]. However, stochastic cooling is not practical for heavy ions because the cooling time is too long. We will therefore discuss our models with respect to electron cooling and laser cooling.

1. Electron cooling

In an electron cooler [22], the electrons are emitted from the surface of a cathode heated to about 1000 K and have a thermal energy spread of $kT_e = kT_{\text{cath}} \sim 100$ meV. These electrons are accelerated to the ion beam velocity and, as a consequence of the acceleration and heating effects, the longitudinal electron temperature is reduced to $kT_{e\parallel} \sim 10^{-4}$ eV [28], while the transverse temperature remains unaffected. An improvement was recently made in the CRYRING electron cooler [29]. The electron beam is guided to the cooling region by a decreasing magnetic field, and its transverse temperature is reduced by a factor of 10 as its size is expanded by the same factor. Finally, an electron beam, with $T_{e\perp} \sim 100$ K and $T_{e\parallel} \sim 1$ K, merges with the hot circulating ion beam over a cooling length of ~ 1.0 m.

The cooling force and cooling time measurements have been performed in a number of electron cooling facilities. With singly charged light ions and the expanded electron beam in the CRYRING cooler [29], a longitudinal cooling force of 2.4 eV/m at a relative velocity of 10^4 m/s and an estimated cooling time of 0.5 s were obtained. With heavy ions, in the TSR electron cooler at Heidelberg, the maximum cooling forces for C^{6+} , Si^{14+} , and S^{16+} ion beams were determined [30] to be 5.5, 7.8, and >40 eV/m, respectively. The accumulation and electron cooling of fully stripped heavy ions from O^{8+} to U^{92+} at energies between 90 and 300 MeV/u has been performed in the ESR storage ring at Darmstadt [31]. The cooling times were found to be 2.4 ms for Ne^{10+} at 150 MeV/u and 0.9 ms for Bi^{82+} at 230 MeV/u, respectively [32].

With the present parameters of the CRYRING cooler, the longitudinal cooling forces are theoretically estimated [33] to be 2.61 eV/m for Li^+ and 844 eV/m for the Ar^{18+} ,

with a temperature limit of 1 K. The cooling time, for a spherical Maxwellian electron velocity distribution, is estimated to be 114 ms for Li^+ and 2 ms for Ar^{18+} .

2. Laser cooling

In laser cooling [26], a photon transfers momentum to an atom as it induces an electronic transition in the atom. The excited atom eventually decays by emission of a photon in a random direction. The excitation-decay cycle gives a net momentum change in the direction of the laser beam. Only a few ion species are suitable for laser cooling, for example, Li^+ , Be^+ , Be^{2+} , Mg^+ , and Er^+ .

At ASTRID Århus [34], a 100-keV Li^+ ion beam, with an initial longitudinal temperature of 100 mK and an initial transverse temperature of 1000 K, was cooled to a longitudinal temperature of 1 mK. In this case, the estimated cooling force was 79 meV/m and the estimated cooling time was 10.5 ms [35]. At TSR in Heidelberg, 10^6 Be^+ ions with energy of 7.3 MeV were cooled to a longitudinal temperature of 5 mK [36]. The estimated cooling force was 223 meV/m and the corresponding cooling time was 3.7 ms [35].

The theoretical limit on the cooling time [37] is of the order of 1 ms. The theoretical limit for the achievable longitudinal temperature is given by the Doppler limit [38]. For the cooling of Li^+ , the useful transition is from 3S_1 to 3P_2 with a Doppler limit of 89 μK . For the cooling of Be^+ , the Doppler limit for the $^2S_{1/2}$ to $^2P_{1/2}$ transition is 440 μK .

D. Ordering parameter

In the studies of an infinitely large three-dimensional system immersed in an oppositely charged uniform background, a dimensionless coupling parameter Γ was introduced, which represents the ratio of the average Coulomb energy to the thermal energy of an ion [39]:

$$\Gamma = \frac{q^2}{4\pi\epsilon_0 a k_B T}, \quad (12)$$

where k_B is the Boltzmann constant, a is the Wigner-Seitz radius defined by $\frac{4}{3}\pi a^3 n_0 \equiv 1$, and n_0 denotes the average particle density of the ion cloud. It was found that a transition from a gaseous to a liquid phase occurs at $\Gamma \approx 10$, whereas $\Gamma \approx 170$ may be associated with a transition from a liquid to a solid phase [39].

In the study of crystallization in infinitely large 2D systems, the 2D coupling parameter Γ and the 2D Wigner-Seitz radius a were adopted from the 3D case [40]. Consistent with the definitions in 3D and 2D situations, we extend the definition of the coupling parameter Γ to the 1D case as

$$\Gamma_{\parallel} = \frac{q^2}{4\pi\epsilon_0 a k_B T_{\parallel}}, \quad (13)$$

where a is the average interparticle distance.

Other ordering parameters introduced earlier are the pair correlation as a function of a spatial coordinate and the mean square displacement as a function of time, yielding a diffusion coefficient. However, in the case of studying the evolution of a system as a function of temperature, where thousands of temperature steps are sampled, it is not practical to use these functions since one plot would be needed for each step. Here we introduce an ordering parameter $C(T)$ as a direct function of temperature or time:

$$C(T(t)) = 1 - \frac{D(T(t))}{\bar{d}(T(t))}, \quad (14)$$

where $D(T(t))$ is the sample standard deviation function:

$$D(T(t)) = \left[\frac{1}{N} \sum_{i=1}^N [d_i(T(t)) - \bar{d}(T(t))]^2 \right]^{\frac{1}{2}}, \quad (15)$$

with \bar{d} as the average value of the interparticle distance $\bar{d}(T(t)) = \frac{1}{N} \sum_{i=1}^N d_i(T(t))$. Here $d_i(T(t))$ is the i th interparticle distance calculated from time averaged positions of ion i and its nearest neighboring ion:

$$d_i(T(t)) = \min_{j \neq i} |\bar{\mathbf{r}}_i - \bar{\mathbf{r}}_j|, \quad j = 1, 2, 3, \dots, N. \quad (16)$$

$C(T)$ depends on neither the choice of the sampling point nor the size of a region. The value of $C(T)$ gives a measure of the ordering of the entire system at temperature T . For a system with an infinite number of randomly distributed particles, $C(T) = 0$; whereas perfect order corresponds to $C(T) = 1$. Due to the boundary conditions in a system of a finite number of particles, the value of $D(T) = 0$ [or $C(T) = 1$] might not be reached even as the temperature approaches zero.

In the case of 1D ordering, it is more important to calculate $C(T)$ as a function of T_{\parallel} . In the 3D case, by restricting the calculation to the ions within one shell, $C(T)$ gives a measure of ordering within that shell; whereas, restricting the calculation to the transverse direction, $C(T)$ gives a measure of ordering between the shells. When all the ions are taken into account, $C(T)$ represents an overall measure of the system ordering.

III. SIMULATION OF CRYRING

As an example of a realistic storage ring, CRYRING at the Manne Siegbahn Laboratory at Stockholm University [41] is chosen for this study. The reason for this selection is that CRYRING, has high symmetry, soft bending, gentle focusing, and smoothly varying β functions, and is therefore one of the most suitable existing storage rings for the investigation of ion beam ordering. The layout of CRYRING is presented in Fig. 2. It is a nearly circular machine with a circumference of 51.63 m, constructed in six superperiods. Each superperiod consists of two rectangular dipoles, three quadrupoles, two sextupoles, two

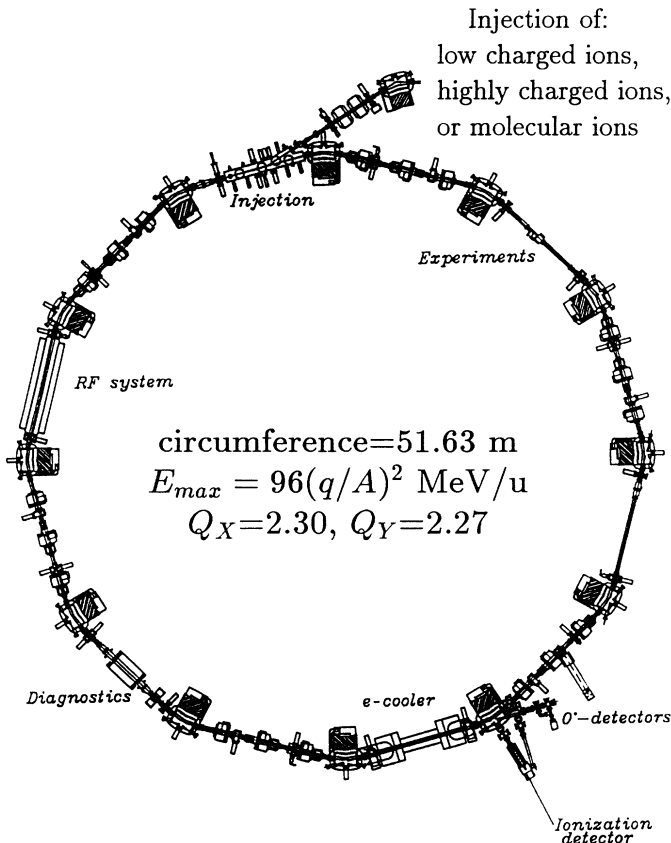


FIG. 2. Layout of the CRYRING facility.

pickups, and two straight sections. Ions, from singly to highly charged, can be injected into the storage ring at low energy (typically 300 keV/u) and accelerated to the desired energy of up to $96(q/A)^2$ MeV/u, where Z and A are the charge and atomic mass numbers of the ions.

An important parameter characterizing an alternating gradient focusing lattice is the tune. The tunes Q_X and Q_Y are the numbers of horizontal and vertical betatron oscillations made by a single particle over a complete circulation of the ring. A pair of Q_X and Q_Y values define a working point for a storage ring. The designed normal working point for CRYRING is at $Q_X = 2.300$ and $Q_Y = 2.270$, which provides stable working conditions for most experiments with heavy ions. The transition to an ordered ion beam requires a suppression of the betatron oscillations as the temperature decreases. According to a study made by Hofmann and Struckmeier [17], the contribution to the tune by each superperiod should not exceed the value of 0.5; otherwise, the matched solution with $Q \rightarrow 0$ due to $T \rightarrow 0$ may not exist. This requires $Q_X, Q_Y < 3.0$ for storage rings with six superperiods, which is satisfied at the normal working point of CRYRING. At this working point, according to the same study [17], some heating is expected since the tunes exceed the safe condition of $Q_X, Q_Y < 1.5$ for macroheating due to the envelope instability. However, this upper limit is not as critical as the preceding condition, since a variation of up to 20% is allowed. We find no severe heating effect caused by the envelope instability at the CRYRING normal working point.

The normal working point of CRYRING is achieved

with the magnetic settings listed in Table I [43]. The $k_X(s)$ and $k_Y(s)$ values expressed by Eq. (3) within a superperiod are displayed in Fig. 3. To check whether the CRYRING lattice is correctly modeled, we compare the tunes obtained from our MD code with both the measured values and those provided by the MAD [42] computer program that was used for the CRYRING design. A single particle orbit was traced in CRYRING with our MD program, and the tunes Q_X, Q_Y were calculated from discrete Fourier transforms of the phase space coordinates. The values of the fractional parts of the tunes obtained from MD are given by the positions of the peaks in Fig. 4, where the arrows indicate the positions of corresponding peaks from MAD. The MD calculation gives the results $Q_X = 2.298$ and $Q_Y = 2.269$, which are in good agreement with the designated values. The MAD

TABLE I. The magnet settings for the normal working point of CRYRING, where the locations are measured from the beginning point of the superperiod to the entrance of the magnets.

Magnets	Location (m)	Length (m)	Strength	
			in x plane (m^{-2})	in y plane (m^{-2})
1st dipole	1.750	0.628	-0.060	2.331
1st quadrupole	2.978	0.300	1.676	-1.676
2nd quadrupole	4.152	0.300	-2.095	2.095
3rd quadrupole	5.326	0.300	1.676	-1.676
2nd dipole	6.226	0.628	-0.060	2.331

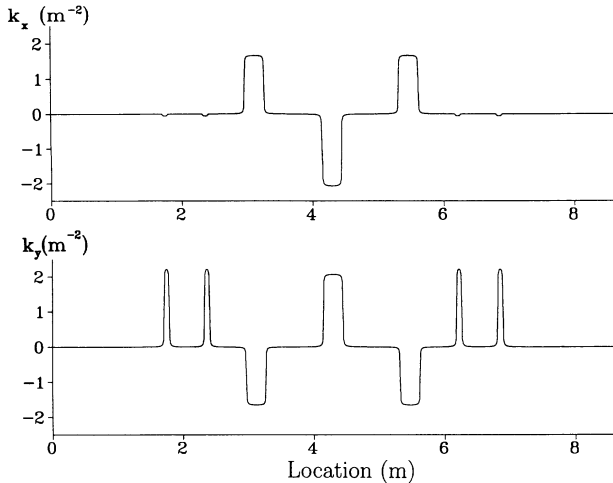


FIG. 3. The $k_X(s)$ and $k_Y(s)$ values, at the normal working point of CRYRING, within a superperiod. All the quadrupole and dipole magnets are taken into account.

predictions have been confirmed by a series of tune measurements at CRYRING. Our tune results indicate that the beam optics of CRYRING is correctly treated in our calculations.

Emittance calculation provides another check of the MD simulations. The emittances ϵ_X and ϵ_Y for a single particle are defined by the area covered by the horizontal and vertical phase space ellipses, respectively. If neither

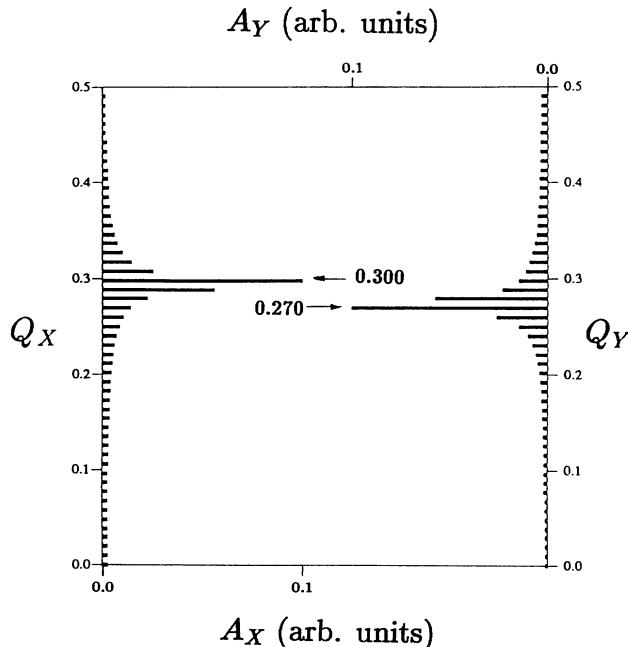


FIG. 4. The horizontal and vertical tunes calculated with the MD code at the normal working point of CRYRING compared with the tunes from the MAD calculation. The values of the fractional parts of the tunes obtained from MD are given by the positions of the peaks. The arrows indicate the positions of corresponding peaks from MAD.

heating nor cooling is applied, emittances are invariant to the variation of location s along the ring, although the shape of the phase space ellipse varies. The calculations of the single particle emittance show that the MD simulation conserves the ϵ_X and ϵ_Y values if heat exchange with an external source is absent.

IV. 1D ORDERING OF ION BEAMS IN CRYRING

A. Initial conditions and simulation parameters

With $N_c \sim 5 \times 10^4$, the simulation of 1D ordering of $N \sim 10^6$ ions in CRYRING is reduced to that of a few tens of ions in the basic cell (Sec. II B). The basic cell has a diameter of 2 cm and a length of $l=0.6$ mm for the case of Li^+ and $l=1.6$ mm for Ar^{18+} . The initial positions of N/N_c ions are generated randomly in the basic cell with a Maxwellian velocity distribution at a specified initial temperature $T(t=0)$ in the moving frame (Sec. II). As a result of the generation of random numbers, the initial position of the center of mass (c.m.) may not coincide with the geometrical center of the basic cell, and the initial velocity of c.m. may differ from zero. Therefore, at the beginning of the simulation, the initial position and velocity of the c.m. are calculated and subtracted from each ion.

The energy of the simulated Li^+ beams was chosen to be 13.3 MeV, since laser cooling of Li^+ beams in CRYRING is planned at this energy following the scheme applied at TSR in Heidelberg [44]. Maintaining the same magnetic rigidity, an energy of 754 MeV is chosen for the simulations of Ar^{18+} beams.

A 1D ordered chain is stable only if the Coulomb repulsion force for a small lateral ion displacement can be compensated by the lattice restoring force. Assuming the storage ring is homogeneously focusing with the average restoring force, Hofmann *et al.* gave a simple estimation of the minimum ion spacing L_{\min} in a 1D string [17]:

$$L \geq L_{\min} \equiv \left(\frac{4Z^2 R^2 r_p}{A\beta^2 \gamma^3 Q_0^2} \right)^{\frac{1}{3}}, \quad (17)$$

where R and Q_0 are machine radius and tune (in the absence of space charge), $\beta \equiv \frac{v_0}{c}$, $\gamma \equiv (1 - \beta^2)^{-1/2}$,

and $r_p \equiv \frac{e^2}{(4\pi\epsilon_0)m_p c^2} \approx 1.535 \times 10^{-18}$ m is the classical proton radius. With the same model Hasse and Schiffer [14] gave analytic and MD results of the critical linear particle density for the transition from 1D ordering to a zigzag configuration, which yields a similar expression (within a factor of 1.017). With the parameters at the normal working point of CRYRING and the ion energies given above, Eq. (17) gives the minimum spacings of $14 \mu\text{m}$ for Li^+ and $25 \mu\text{m}$ for Ar^{18+} beams, which yield maximum ion numbers of 3.7×10^6 and 2.1×10^6 , respectively. Our MD simulations showed that the maximum ion numbers for which linear chains formed in CRYRING

were 1.4×10^6 for Li^+ and 5.5×10^5 for Ar^{18+} system. It seems that a factor of ~ 0.3 is needed in expression (17) when the homogeneous focusing is replaced by alternating gradient focusing. In this work, 1.377×10^6 and 5.486×10^5 were chosen as the total number of ions for Li^+ and Ar^{18+} systems, respectively.

The step size δt remains constant throughout the simulations with $\delta t=52.29$ ps for Li^+ and $\delta t=16.58$ ps for Ar^{18+} . During the intervals δt , the basic cell traverses 1.0 mm along CRYRING at the beam velocity. This distance is small compared to the typical length over which the external fields vary. When the basic cell passes through the cooling section, the operation described by Eq. (9) is applied. The effective cooling length is 1.0 m, which is equal to the length of the CRYRING electron cooler. A similar length can be expected for laser cooling. The time evolutions of the Li^+ ion beams were simulated for 5.229 ms, while Ar^{18+} ion beams were followed for a total time of 1.658 ms. The positions and velocities of the ions were sampled at the entrance position of the first super-period in CRYRING. From this information the longitudinal and transverse temperatures, as well as Γ_{\parallel} , were calculated.

B. Cooling parameters

In Table II we display the cooling parameters used in our MD simulations and the values expected from electron and laser cooling. It is generally desirable to choose MD cooling parameters to be as close as possible to the values obtained either from experimental measurements or theoretical estimates. However, it is not possible to perform a MD simulation for such a long cooling time due to limitations of CPU time. The feasible cooling time in our MD simulation is of the order of 0.1 ms, which is about 20 times faster than the estimated cooling time for Ar^{18+} and about 100 times faster than the one for Li^+ . To confirm that the simulation results are still valid with the faster cooling, it was carefully checked that the cooling is slow enough to ensure thermal equilibrium in both the longitudinal and transverse directions during the simulations. As discussed above, the heating due to envelope instability was not observed as well. In our MD simulations, $100 \mu\text{K}$ was chosen to be the temperature limit for the Li^+ beam, which is close to the Doppler limit of $89 \mu\text{K}$ by laser cooling. For the Ar^{18+} beam there is still a large difference between the estimated temperature limit and the one used in our MD simulations. The necessary temperature to achieve a well-ordered structure ($\Gamma \sim 10^3$) is around 50 mK, while the experimental temperature limit is 930 mK, which is the lowest electron temperature cur-

TABLE II. Comparison of the cooling parameters in MD simulations and the expected values.

Cooling parameter	Electron cooling	Laser cooling
	Ar^{18+}	Li^+
Estimated cooling time	2.0 ms	10.5 ms
MD cooling time (uniform)	0.11 ms	0.13 ms
MD cooling time (longit.)	0.12 ms	0.24 ms
Estimated temperature limit	930 mK	89 μK
MD temperature limit	50 mK	100 μK

rently reached in the CRYRING electron cooler. This limit is continually being lowered with improvements in electron cooling technology.

C. 1D ordering of Li^+ beams

1. Longitudinal cooling

The heat exchange among different degrees of freedom in dilute beams, which are in the initial stage cold longitudinally and warm transversally, has been studied in idealized storage rings [52,53]. In this section, we investigate the coupling between longitudinal and transverse ion motions and the ordering effect in a realistic CRYRING lattice, where longitudinal cooling is applied to a beam that is initially warm in all degrees of freedom. Such a case could be realized by laser cooling where no direct cooling of the transverse ion motion occurs (Sec. II C 2). The longitudinal cooling parameters used in the simulation are listed in Table III.

To visualize how the system becomes ordered, the ion positions of the three-dimensional system are plotted in two-dimensional (z, r) diagrams, where $r_i = \sqrt{x_i^2 + y_i^2}$ is the displacement of the i th ion from the center of the beam. Figure 5 provides an overview of the transition of the system from a random to an ordered phase as the longitudinal temperature decreases. In Fig. 5(a), the system is completely random with a high longitudinal temperature of 182 K. In Fig. 5(b), T_{\parallel} is reduced to 10 K, the system is still disordered. One can see from Fig. 5(c) that, at $T_{\parallel}=20$ mK, the random motions are reduced and the ions stop passing each other longitudinally. The ion motions shown in Fig. 5(d) indicate that the Coulomb potential energy becomes significant compared to the thermal energy of the ions at $T_{\parallel}=1$ mK. During this stage, the ions remain separated longitudinally from each other while they oscillate around their equilibrium positions with large transverse amplitudes. At $T_{\parallel}=0.1$ mK, a linear ordered structure can easily be observed [Fig. 5(e)]. The longitudinal ion motions are small compared to the mean interparticle distance, whereas the transverse ion excursions are almost unchanged. The stable beam envelope has nodes (i.e., where the ions have small transverse displacements and large transverse velocities) at the center of the straight sections. Notice that all (z, r) plots are made at the center of one of the straight sections and the

TABLE III. The cooling parameters used in the simulations of the Li^+ beam.

Cooling parameter	Longitudinal	Uniform
Initial longitudinal temperature T_{\parallel}	45 kK	45 kK
Initial transverse temperature T_{\perp}	202 kK	202 kK
Desired longitudinal temperature T_{\parallel}^c	0.10 mK	0.10 mK
Desired transverse temperature T_{\perp}^c		0.10 mK
Longitudinal cooling strength γ_{\parallel}	$0.50 \mu\text{s}^{-1}$	$0.50 \mu\text{s}^{-1}$
Transverse cooling strength γ_{\perp}		$0.50 \mu\text{s}^{-1}$
Effective longitudinal cooling time τ_{\parallel}	0.24 ms	0.13 ms
Effective transverse cooling time τ_{\perp}		0.16 ms

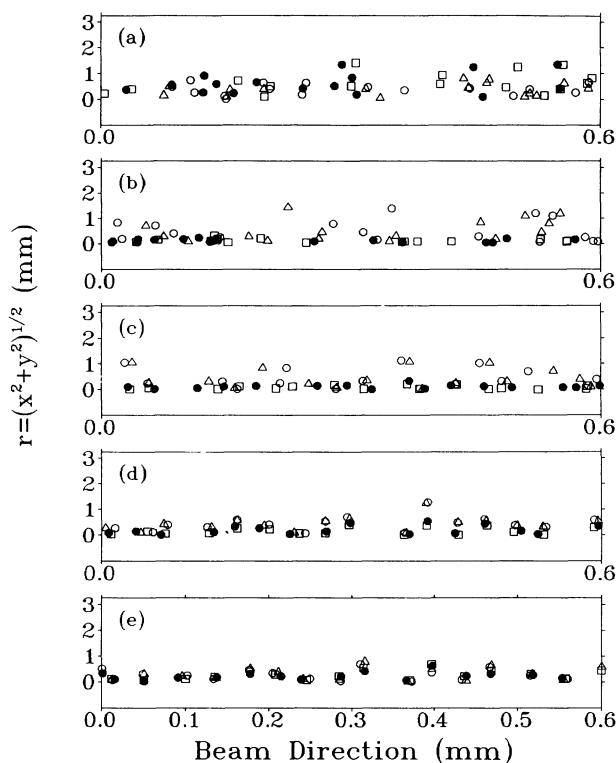


FIG. 5. The full dots are the (z, r) positions of the Li^+ system at five different stages during longitudinal cooling. The open triangles, squares, and circles give the distributions after 1, 2, and 3 circulations around the ring. (a) at $t = 1.1$ ms, $T_{||} = 182$ K, $T_{\perp} = 214$ kK, and $\Gamma_{||} = 1 \times 10^{-4}$; (b) at $t = 1.4$ ms, $T_{||} = 10$ K, $T_{\perp} = 214$ kK, and $\Gamma_{||} = 2 \times 10^{-3}$; (c) at $t = 1.9$ ms, $T_{||} = 20$ mK, $T_{\perp} = 214$ kK, and $\Gamma_{||} = 1$; (d) at $t = 2.1$ ms, $T_{||} = 1$ mK, $T_{\perp} = 214$ kK, and $\Gamma_{||} = 50$; (e) at $t = 2.9$ ms, $T_{||} = 0.1$ mK, $T_{\perp} = 214$ kK, and $\Gamma_{||} = 500$.

transverse scales are compressed compared to the longitudinal ones.

The values of $T_{||}$, T_{\perp} , and $\Gamma_{||}$ as functions of time are displayed in Fig. 6, from which several observations can be made. First, both $T_{||}$ and $\Gamma_{||}$ vary smoothly and almost exponentially from their initial values toward asymptotic limit. This behavior is governed by the cooling characteristic described in Eq. (9). There is no structure of an ordering transition visible. Second, the initial transverse temperature is five times higher than the initial longitudinal temperature, even though the initial ion velocities were generated with the same width in all dimensions in the moving frame. The reason for this is that the large lateral spread of the initial position distribution contributes to the transverse emittance. Third, from its initial value, the longitudinal temperature slowly approaches the specified cooling limit, in this case $T_{||}^c = 0.10$ mK (Table III), while the system remains hot transversally and retains at its initial T_{\perp} value. This indicates that, with the selected ion densities, the coupling of longitudinal and transverse motions is weak.

The ordering parameter $C(T)$ is displayed in Fig. 7. The $\Gamma_{||}$ scale on the top of the figure is deduced from Eq. (13) assuming a constant particle density. By exam-

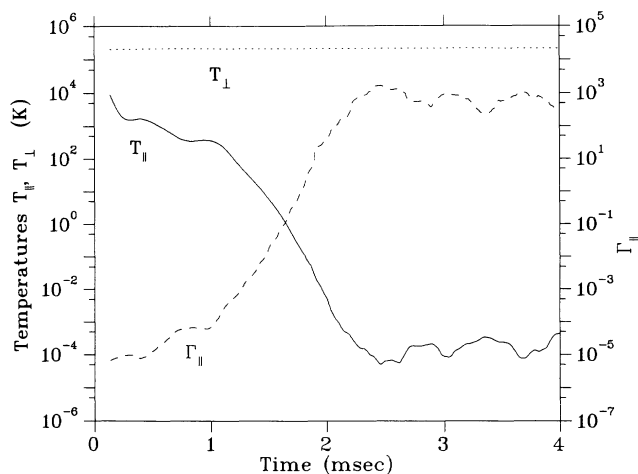


FIG. 6. The values of $T_{||}$, T_{\perp} , and $\Gamma_{||}$ of the Li^+ system versus time during longitudinal cooling.

ining Figs. 5–7 one finds that it is advantageous to use $C(T)$ for determining the temperature at which ordering occurs. $C(T)$ has no temperature dependence and maintains a low value around 0.1 (Fig. 7) when the system is in a random state [Fig. 5(a)] during the initial stage of cooling, i.e., at $T_{||} > 5$ K. For a longitudinal temperature close to $T_{||} = 1$ K, $C(T)$ starts to increase, indicating that the ions start to order themselves. Figure 5(b) represents the system before this initial phase of ordering. $C(T)$ keeps increasing as the longitudinal temperature is further reduced. At $T_{||} = 10$ mK, $C(T)$ becomes 0.5, and the system is partially ordered [Fig. 5(c)]. When $T_{||}$ decreases to 1 mK and $\Gamma_{||}$ increases to 50, $C(T)$ reaches 0.6, which is the degree of ordering in the system at the cooling stage shown in Fig. 5(d). As $T_{||}$ falls below 1 mK, $C(T)$ starts to approach its asymptotic value of 0.62, indicating that the ordering is no longer significantly improving, as presented by Fig. 5(e), which is a measure of the system ordering in its final state.

The above example suggests that $C(T)$ is a useful

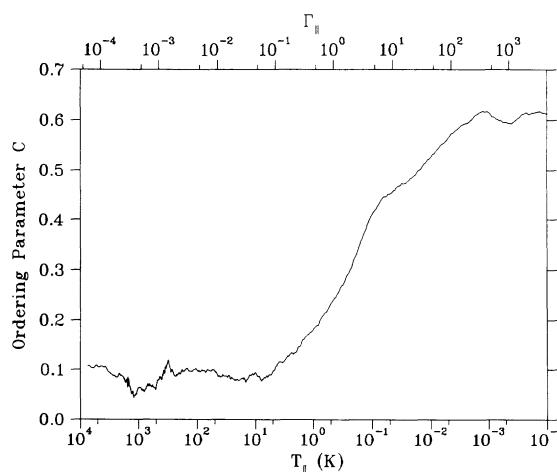


FIG. 7. The ordering parameter C of the Li^+ system as a function of $T_{||}$ and $\Gamma_{||}$ during longitudinal cooling.

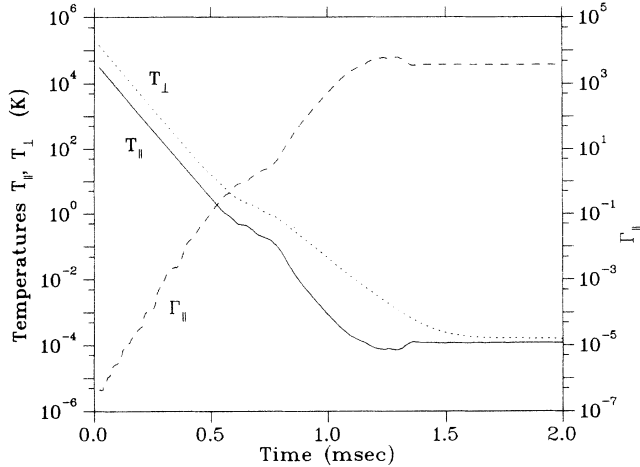


FIG. 8. The values of T_{\parallel} , T_{\perp} , and Γ_{\parallel} of the Li^+ system versus time during uniform cooling.

parameter that indicates the temperature range within which the ordering in the system occurs. The asymptotic value of $C(T)$ shows the degree of ordering that can be achieved, with a cooling rate applied in a specific system.

2. Uniform cooling

In this section, we determine the degree of ordering that could be obtained in the same system with transverse cooling as strong as longitudinal cooling. The study of uniform cooling is also interesting from the viewpoint of heat dissipation from longitudinal and transverse degrees of freedom. Even with the same longitudinal and transverse cooling forces, the asymptotic ion temperatures can differ. A simulation was done with the uniform cooling parameters listed in Table III.

The T_{\parallel} , T_{\perp} , and Γ_{\parallel} values of the Li^+ system during uniform cooling are displayed in Fig. 8. Some similarities to the case of longitudinal cooling are seen by comparing

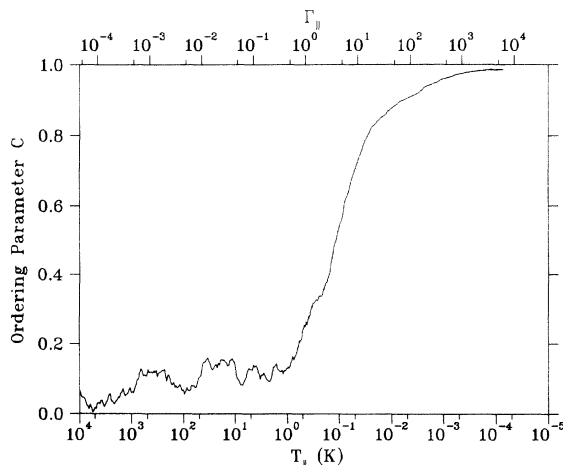


FIG. 9. The ordering parameter C of the Li^+ system as a function of T_{\perp} and Γ_{\parallel} during uniform cooling.

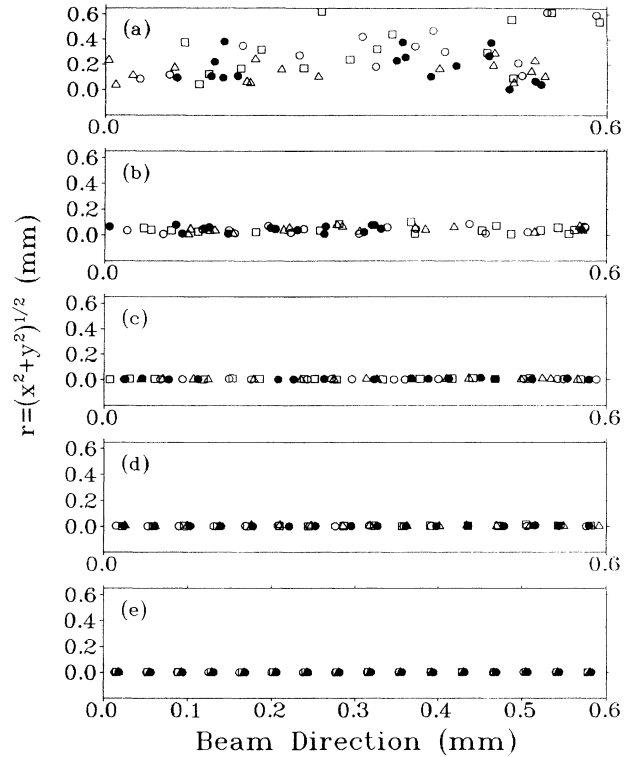


FIG. 10. The full dots are the (z, r) positions of the Li^+ system at five different stages during uniform cooling. The open triangles, squares, and circles give the distributions after 1, 2, and 3 circulations around the ring. (a) at $t = 0.2$ ms, $T_{\parallel}=1$ kK, $T_{\perp}=6$ kK, and $\Gamma_{\parallel}=6 \times 10^{-5}$; (b) at $t = 0.4$ ms, $T_{\parallel}=12$ K, $T_{\perp}=55$ K, and $\Gamma_{\parallel}=0.02$; (c) at $t = 0.8$ ms, $T_{\parallel}=88$ mK, $T_{\perp}=0.7$ K, and $\Gamma_{\parallel}=5$; (d) at $t = 0.9$ ms, $T_{\parallel}=5$ mK, $T_{\perp}=0.1$ K, and $\Gamma_{\parallel}=90$; (e) at $t = 1.9$ ms, $T_{\parallel}=T_{\perp}=0.1$ mK, and $\Gamma_{\parallel}=3598$.

Fig. 8 with Fig. 6. Due to uniform cooling T_{\perp} decreases simultaneously with T_{\parallel} . However, T_{\parallel} decreases faster than T_{\perp} , even though equal cooling strengths $\gamma_{\parallel} = \gamma_{\perp}$ (Table III) are applied. This result indicates that it is easier to cool a beam longitudinally than transversally in a storage ring.

In Fig. 9, we display $C(T)$ as a function of T_{\parallel} (and Γ_{\parallel}). Comparing Fig. 9 with Fig. 7, one sees that the ordering transition is more pronounced under uniform cooling. During the first stage of cooling, T_{\parallel} varies over the wide range from 45 kK to 1 K, but $C(T)$ does not alter at all and maintains a low value around 0.1. Figure 10(a) shows the system at this stage of disorder, where $T_{\parallel}=1$ kK and $C(T)=0.1$. As T_{\parallel} reaches 1K, $C(T)$ starts to increase rapidly, indicating that the ions are starting to order themselves [Fig. 10(b) at $T_{\parallel}=12$ K]. When $C(T)$ reaches a value of 0.5 at $T_{\parallel}=88$ mK, the system is partially ordered, as seen from Fig. 10(c). When $C(T)$ becomes 0.9, an ordered chain is clearly visible in Fig. 10(d) ($T_{\parallel}=5$ mK). Finally, the system emerges as a well-ordered one when $C(T)$ is close to 1 [Fig. 10(e)], at $T_{\parallel}=0.1$ mK and $\Gamma_{\parallel}=3598$. We conclude that uniform cooling provides higher values of $C(T)$ and Γ_{\parallel} than in the case of longitudinal cooling only.

D. 1D ordering of Ar^{18+} beams

Highly charged ions give a much higher Γ value than singly charged ions at the same temperature and density. However, the intrabeam scattering growth rate increases with q^4 [45]. The lowest achievable ion temperature is determined by a balance between the applied cooling rate and the heating rate. In this section, we choose Ar^{18+} to study the temperature dependence of a highly charged ion system. Comparing Ar^{18+} with the Li^+ system under similar cooling conditions, we study similarities and differences in ordering due to the ion charge state.

The only cooling mechanism for highly charged ions is, at present, electron cooling. The cooling force, cooling time, and the ion temperature limit depend strongly on the electron temperature. In the CRYRING electron cooler, the current electron temperatures are $k_B T_{\parallel} \approx 0.1$ meV and $k_B T_{\perp} \approx 10$ meV [29]. A further improvement to reduce the transverse electron temperature to 1 meV is planned [46]. Smaller differences between transverse and longitudinal electron temperatures can thus be expected with continuous improvement in electron cooling technology. This may finally allow cooling of both the longitudinal and transverse ion motions with comparable strengths. The uniform cooling parameters used in this section are listed in Table IV.

The values of T_{\parallel} , T_{\perp} , and Γ_{\parallel} , as functions of time during uniform cooling of the Ar^{18+} system, are displayed in Fig. 11. The properties of T_{\parallel} and Γ_{\parallel} observed in the singly charged ion system (Fig. 8) are also seen in this highly charged ion system. The ordering parameter $C(T)$ as a function of T_{\parallel} (or Γ_{\parallel}) for the Ar^{18+} system during uniform cooling is shown in Fig. 12. When T_{\parallel} is reduced from 11 kK to 200 K, $C(T)$ fluctuates around 0.1 showing no temperature (or Γ_{\parallel}) dependence over this wide range. The system is still disordered, as seen in Fig. 13(a) (at $T_{\parallel}=11$ kK). As T_{\parallel} approaches 200 K, $C(T)$ starts to increase indicating that the ions are beginning to order themselves. At this initial stage of ordering, seen in Fig. 13(b) for $T_{\parallel}=200$ K, the beam size has been reduced. When $C(T)$ reaches a value of 0.5, as in Fig. 13(c) ($T_{\parallel}=15$ K), the system is partially ordered. When $C(T)$ becomes 0.9, ordering is clearly visible from Fig. 13(d) ($T_{\parallel}=1$ K). The final stage of cooling, with $C(T)$ as high as 0.98, is shown in Fig. 13(e) ($T_{\parallel}=25$ mK).

The temperatures for ordering transitions are dependent strongly on the charge state (Figs. 13 and 10). The ordering transition starts around 200 K and ends around

TABLE IV. The cooling parameters used in the simulations of Ar^{18+} beams.

Cooling parameter	Longitudinal	Uniform
Initial longitudinal temperature T_{\parallel}	11 kK	11 kK
Initial transverse temperature T_{\perp}	70 kK	70 kK
Desired longitudinal temperature T_{\parallel}^c	50 mK	50 mK
Desired transverse temperature T_{\perp}^c		50 mK
Longitudinal cooling strength γ_{\parallel}	$0.45 \mu\text{s}^{-1}$	$0.45 \mu\text{s}^{-1}$
Transverse cooling strength γ_{\perp}		$0.45 \mu\text{s}^{-1}$
Effective longitudinal cooling time τ_{\parallel}	0.12 ms	0.11 ms
Effective transverse cooling time τ_{\perp}		0.17 ms

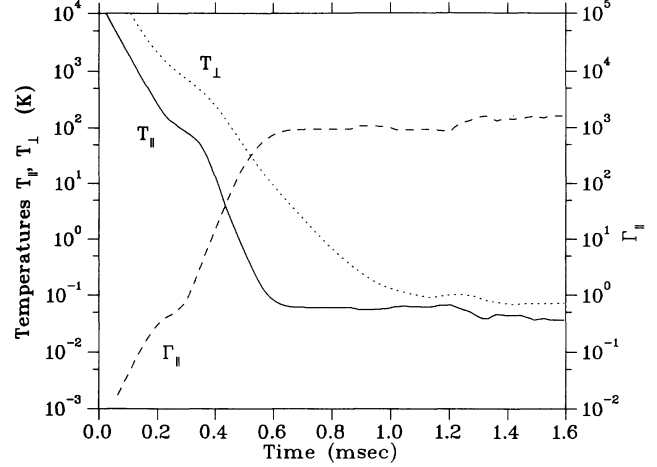


FIG. 11. The values of T_{\parallel} , T_{\perp} , and Γ_{\parallel} of the Ar^{18+} system versus time during uniform cooling.

1 K in the Ar^{18+} case, while the Li^+ system starts ordering around 1 K and ends around $T_{\parallel}=1$ mK. Notice that the corresponding Γ_{\parallel} values are about 0.3 and 50, respectively, in both cases. Comparing the asymptotic value of $C(T)$ obtained in the Ar^{18+} system with the one obtained in the Li^+ system, it can be seen that both species would reach the same degree of ordering [$C(T)=0.98$] if they have similar final Γ_{\parallel} values [$\Gamma_{\parallel} = (2 - 4) \times 10^3$].

In order to see to what degree longitudinal and transverse temperatures equilibrate by intrabeam scattering in highly charged ions, longitudinal cooling of Ar^{18+} was also investigated. Most of the features seen for longitudinal cooling of Li^+ remain in the highly charged ion system. The ordering transition occurs again around $T_{\parallel} \sim 200$ K in the Ar^{18+} case, while the Li^+ system starts to show 1D ordering at $T_{\parallel}=1$ K. The corresponding Γ_{\parallel} values are about 0.3 in both cases. A linearly ordered structure was also observed in this longitudinally cold ($T_{\parallel}=50$ mK), but transversely hot [$T_{\perp}=70$ kK], highly charged ion system.

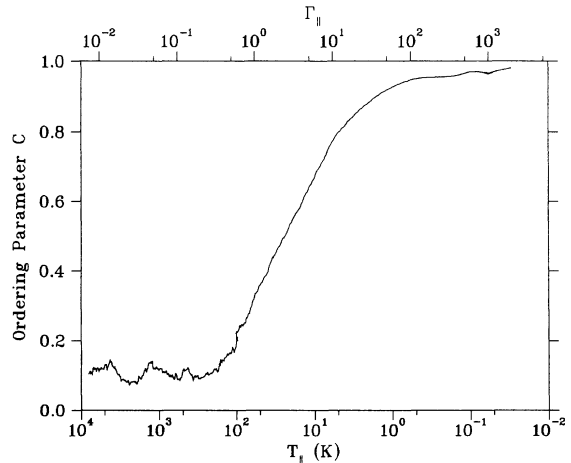


FIG. 12. The ordering parameter C of the Ar^{18+} system as a function of T_{\parallel} and Γ_{\parallel} during uniform cooling.

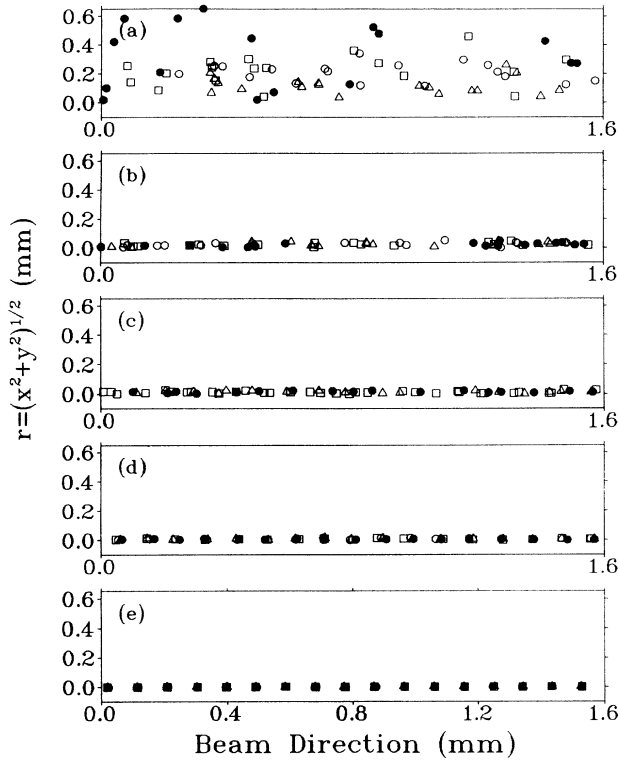


FIG. 13. The full dots are the (z, r) positions of the Ar^{18+} system at five different stages during uniform cooling. The open triangles, squares, and circles give the distributions after 1, 2, and 3 circulations around the ring. (a) at $t = 0.001$ ms, $T_{\parallel} = 11$ kK, $T_{\perp} = 68$ kK, and $\Gamma_{\parallel} = 3 \times 10^{-3}$; (b) at $t = 0.2$ ms, $T_{\parallel} = 200$ K, $T_{\perp} = 2$ kK, and $\Gamma_{\parallel} = 0.3$; (c) at $t = 0.4$ ms, $T_{\parallel} = 15$ K, $T_{\perp} = 360$ K, and $\Gamma_{\parallel} = 3$; (d) at $t = 0.5$ ms, $T_{\parallel} = 1$ K, $T_{\perp} = 80$ K, and $\Gamma_{\parallel} = 50$; (e) at $t = 1.3$ ms, $T_{\parallel} = 25$ mK, $T_{\perp} = 90$ mK, and $\Gamma_{\parallel} = 2069$.

V. DETECTION OF 1D ORDERING USING A SCHOTTKY NOISE DETECTOR

One of the main diagnostic instruments in a storage ring is the Schottky detector [47], which consists of four equal-size plates placed symmetrically around the beam axis. As the ions pass the Schottky detector, they induce image charges in the plates and generate pulse signals in the amplifier. One can determine the positions of ions by taking the proper differences of the signals from the individual plates, and obtain information related to the passage of the ions in the time domain by taking the sum of the signals. To detect 1D ordered beams, we shall be mainly interested in this timing information.

At a very low temperature, the ions of an ideal 1D ordered system perform macro oscillations around their equilibrium positions equally spaced along the central orbit. If the longitudinal motion can be separated from the transverse motion and the oscillation amplitudes are small compared to the spacing between the ions, the system can be treated as a closed chain of N coupled harmonic oscillators with equal interparticle distance, and

the phonon approximation can be used for the description of the system. The longitudinal Schottky spectrum has been studied analytically [48,53] with this idealized 1D model.

In our study, longitudinal Schottky noise was extracted from the MD data by simulating the Gaussian shaped pulse signal induced by the passage of each ion through a pickup detector located in the middle of a drift section, i.e., the starting point of a superperiod of CRYRING. Fast Fourier transforms were performed on these simu-

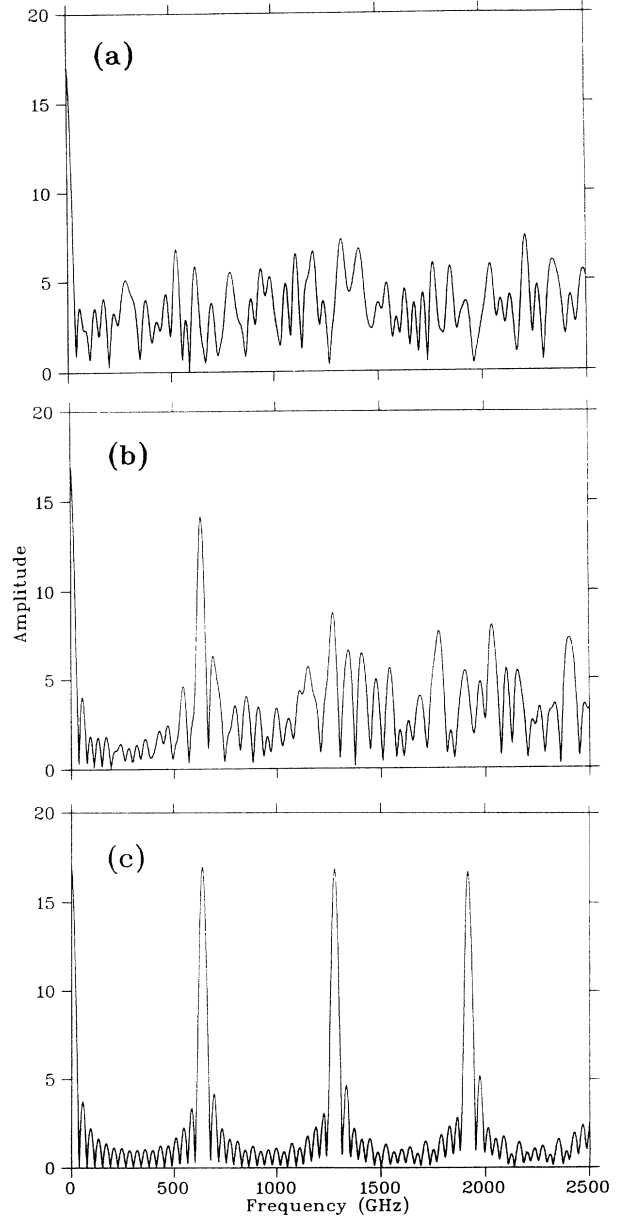


FIG. 14. An example of a high-frequency Schottky spectra. (a) There is no peak at 641 GHz since the system is not ordered or only partially ordered; see Fig. 13(c). (b) The peak at 641 GHz becomes clearly visible when an ordering structure becomes apparent, see Fig. 13(d). (c) The peak at 641 GHz and its harmonics are dominant as the beam is ultracooled and an ordered structure is well formed; see Fig. 13(e).

lated signals to obtain the frequency spectra.

Many theoretical studies and experimental observations of the Schottky spectra are done in the region of frequencies at which ion beams circulate in the ring (on the order of 10^5 Hz) [49]. Unfortunately, the spectra obtained from our MD data do not contain beam information in this frequency region because, as pointed out in Sec. II B, the basic cell model does not include any oscillation modes with wavelengths longer than the length of the basic cell. The middle-frequency spectral lines occur typically around 10^{10} Hz at which, in our simulation, the identical cells pass the detector and create additional periodic signals. Obviously, this frequency is artificially introduced into the simulation by periodic boundary conditions (Sec. II B). The high-frequency region consists of the main spectral line at 10^{11} Hz and its higher harmonics, which are caused by the detection of every single ion in the crystal lattice. If detectable, this lines could give direct evidence of the 1D crystal formation. However, the frequency is too high for detection with existing techniques, although, recently, there have been some investigations into possible narrow-band pickups beyond 10^{11} Hz [50]. Here, the spectra in this frequency region are presented for completeness and for simulation diagnostics.

As an example of the results from the simulation of longitudinal Schottky spectra we show, in Fig. 14, the case of the Ar^{18+} beam at the three different uniform cooling stages corresponding to Figs. 13(c–e), respectively. The frequency of the main spectral line is determined by the crystal lattice constant and the velocity of the beam. Its value is 641 GHz in this case. When $T_{\parallel} > 15$ K there is no peak at 641 GHz [Fig. 14(a)] as the system is not ordered [see Figs. 13(a,b)] or only partially ordered [Fig. 13(c)]. The peak at 641 GHz becomes discernable, as shown in Fig. 14(b), when $T_{\parallel} \sim 1$ K and the ordering in the system becomes apparent [Fig. 13(d)]. When $T_{\parallel} \sim 50$ mK and an ordered structure is well formed [Fig. 13(e)], the peak at 641 GHz and its harmonics become clearly visible; see Fig. 14(c). The amplitude of these lines decreases following a Gaussian shaped envelope that has a standard deviation $1/\sigma_t$, where σ_t is the width of the pulses in the time domain. At this stage, the noise is largely reduced; the small peak at 37.7 GHz and its higher harmonics are also shown in the spectrum. These small peaks are the middle-frequency spectral lines created by the passage of the basic cells through the detector.

VI. CONCLUSIONS AND DISCUSSIONS

We have presented here a method for realistic simulations of ion beam motions in a cooler storage ring including all magnetic elements, fringe fields, shear effect and dispersion. An ordering parameter that characterizes the ordering of ions as a function of T was introduced. We studied the cases of low particle density where 1D ordering could be expected in the Stockholm storage ring—CRYRING lattice. Four sets of simulation of ordering processes, including singly and highly charged ions under longitudinal and uniform cooling, were presented.

Three temperatures could be found at the points where the ordering transition starts, reaches its peak, and finishes. The values of these three temperatures vary from system to system, but they can be easily identified from the $C(T)$ curve of the system. Ordering parameter $C(T)$ starts to increase around 1 K for the Li^+ and 200 K for the Ar^{18+} , both for longitudinal and uniform cooling. In most cases, the corresponding Γ_{\parallel} are around 0.3. The temperature at which dC/dT_{\parallel} reaches its maximum, i.e., the ordering develops in the fastest fashion versus the temperature change, is ~ 50 mK for Li^+ and ~ 20 K for Ar^{18+} . The corresponding Γ values are around 3 while $C(T) \approx 0.5$, which is an indication of a partially ordered system. Ordering continues with decreasing T_{\parallel} , until $C(T)$ is close to its asymptotic value, at which the ordering transition finishes. In the cases investigated, this occurs at ~ 1 mK for Li^+ and ~ 1 K for Ar^{18+} . The corresponding Γ values in all the cases are around 100 or higher. The asymptotic $C(T)$ values are 0.62 for Li^+ with longitudinal cooling and above 0.9 for all other cases.

The critical Γ values obtained here do not agree exactly with the prediction made for a strongly coupled one component plasma of $\Gamma_{\text{crit}} \approx 170$ [39]. This could be due to the size of the system and the external confinement forces in the storage ring, as Γ_{crit} was derived for a 3D infinitely large system immersed in an oppositely charged uniform background.

Longitudinal cooling may be sufficient to obtain 1D ordered chains in both singly or highly charged ion systems if the particle density is small, so that the coupling of the longitudinal and transverse motions is weak. In this case, the longitudinal temperature can be reduced nearly to the cooling limit while the system stays hot transversally.

The results with uniform cooling show that even with the same cooling strengths, the longitudinal and transverse temperatures decrease at different rates and the longitudinal temperature approaches a lower asymptotic value. This behavior is the same for Ar^{18+} and Li^+ with differences in the asymptotic values of temperatures and the cooling rates, i.e., cooling times.

Finally, the Schottky analysis as a tool for observing 1D ordering is studied. The calculated spectra show spectral lines appear at high frequency when 1D ordering occurs, at a multiple of the circulation frequency with the number of stored ions, and higher harmonics. If detectable, these lines could give direct evidence of the 1D crystal formation. However, with practical values of ion numbers and velocities, this frequency is not accessible with the current frequency analysis techniques.

ACKNOWLEDGMENTS

These simulations were based on a general molecular dynamics code [51]. The main program and major sub-routines were rewritten for our particular needs. We acknowledge Professor Orlando Tapia for giving and introducing to us the original code. We are also grateful to the Knut and Alice Wallenberg Foundation for a computer grant necessary for this work.

- [1] R. Schuch, in *Review of Fundamental Processes and Applications of Atoms and Ions*, edited by C. D. Lin (World Scientific, Singapore, 1993), p. 169.
- [2] H. Poth *et al.*, *Z. Phys. A* **332**, 171 (1989).
- [3] J. P. Schiffer and P. Kienle, *Z. Phys. A* **321**, 181 (1985).
- [4] See, for example, GSI Report No. GSI-89-10, 1989 (unpublished).
- [5] R. F. Wuerker, H. Shelton, and R. V. Langmuir, *J. Appl. Phys.* **30**, 342 (1959).
- [6] See, for example, F. Diedrich *et al.*, *Phys. Rev. Lett.* **59**, 2931 (1987); D. J. Wineland *et al.*, *ibid.* **59**, 2935 (1987); R. Blümel *et al.*, *Nature* **334**, 309 (1988); J. Hoffnagle *et al.*, *Phys. Rev. Lett.* **61**, 255 (1988).
- [7] See, for example, S. L. Gilbert, J. J. Bollinger, and D. J. Wineland, *Phys. Rev. Lett.* **60**, 2022 (1988).
- [8] I. Waki, S. Kassner, G. Birkl, and H. Walther, *Phys. Rev. Lett.* **68**, 2007 (1992); G. Birkl, S. Kassner, and H. Walther, *Nature* **357**, 310 (1992).
- [9] E. N. Dementiev *et al.*, *Sov. Phys. Tech. Phys.* **25**, 1001 (1980).
- [10] N. S. Dikansky and D. V. Pestrikov, KfK Report No. 3846, 1984 (unpublished).
- [11] A. Rahman and J. P. Schiffer, *Phys. Rev. Lett.* **57**, 1133 (1986).
- [12] A. Rahman and J. P. Schiffer, *Phys. Scr.* **T22**, 133 (1988).
- [13] J. P. Schiffer, *Phys. Rev. Lett.* **61**, 1843 (1988); R. W. Hasse, *ibid.* **67**, 600 (1991).
- [14] R. W. Hasse and J. P. Schiffer, *Ann. Phys.* **203**, 419 (1990); R. W. Hasse, GSI Report No. GSI-90-23, 1990 (unpublished).
- [15] D. Habs, MPI Report MPI H-1987-V10, 1987 (unpublished).
- [16] J. P. Schiffer and A. Rahman, *Z. Phys. A* **331**, 71 (1988).
- [17] I. Hoffmann, J. Struckmeier, and S. Cocher (unpublished); I. Hoffmann and J. Struckmeier, in [4].
- [18] J. Beebe-Wang, N. Elander, and R. Schuch, in *Proceedings of the 5th International Symposium on Electron Beam Ion Sources and Their Applications, Dubna, USSR, 1991*, edited by E. D. Donets and I. P. Yudin (Publishing Group/Scientific Research Firm "I.V.K.-SOFT", Dubna, Russia, 1992); *Nucl. Instrum. Methods Phys. Res. Sect. B* **79**, 806 (1993).
- [19] J. Wei, X.-P. Li, and A. M. Sessler (unpublished); in CERN Report No. 94-03, 1994 (unpublished).
- [20] D. W. Heermann, *Computer Simulation Methods in Theoretical Physics* (Springer-Verlag, Berlin, 1986), p. 13.
- [21] M. P. Allen and D. J. Tildesley, *Computer Simulation of Liquids* (Oxford University Press, Oxford, 1989), p. 78.
- [22] H. Poth, *Phys. Rep.* **196** (3&4), 135 (1990).
- [23] S. Humphries, *Principles of Charged Particle Acceleration* (John Wiley & Sons, New York, 1986).
- [24] P. Ewald, *Ann. Phys.* **64**, 253 (1921).
- [25] H. J. C. Berendsen *et al.*, *J. Chem. Phys.* **81**, 3684 (1984).
- [26] *J. Opt. Soc. Am. B* **6**, 2020 (1989), special issue on laser cooling.
- [27] D. Möhl, in *Proceedings of CERN Accelerator School*, CERN Report No. 87-03 (CERN, Geneva, 1987), p. 453.
- [28] D. R. DeWitt *et al.*, *Phys. Rev. A* **50**, 1257 (1994).
- [29] H. Danared, in CERN Report No. 94-03, 1994 (unpublished).
- [30] M. Steck *et al.*, in *Proceedings of the Workshop on Electron Cooling and New Cooling Techniques*, edited by R. Calabrese and L. Tecchio (World Scientific, Singapore, 1991), p. 64.
- [31] B. Franzke *et al.* (unpublished).
- [32] M. Steck *et al.* (unpublished).
- [33] Y. Derbenev and A. N. Skrinsky, *Part. Accel.* **8**, 1 (1977).
- [34] J. S. Hangst *et al.*, *Phys. Rev. Lett.* **67**, 1238 (1991).
- [35] G. Bisoffix (unpublished).
- [36] R. Grimm, in CERN Report No. 94-03, 1994 (unpublished).
- [37] S. Stenholm, *Rev. Mod. Phys.* **58**, 699 (1986).
- [38] V. S. Letokhov and V. G. Minogin, *Phys. Rep.* **73** (1), 1 (1981).
- [39] See, for example, S. G. Brush, H. L. Sahlin, and E. Teller, *J. Chem. Phys.* **45**, 2102 (1966); J. P. Hansen, *ibid.* **8**, 3096 (1973); E. L. Pollock and J. P. Hansen, *Phys. Rev. A* **8**, 3110 (1973); J. H. Malmberg and T. M. O'Neil, *Phys. Rev. Lett.* **39**, 1333 (1977); W. L. Slattery, G. D. Doolen, and H. E. DeWitt, *Phys. Rev. A* **21**, 2087 (1980).
- [40] See, for example, R. W. Hockney and T. R. Brown, *J. Phys. C* **8**, 1813 (1975); R. C. Gann, S. Chakravarty, and G. V. Chester, *Phys. Rev. B* **20**, 326 (1979); R. H. Morf, *Phys. Rev. Lett.* **43**, 931 (1979); R. K. Kalia, P. Vashishta, and S. W. de Leeuw, *Phys. Rev. B* **23**, 4794 (1981).
- [41] C.-J. Herrlander, A. Bárány, K.-G. Rensfelt, and J. Starker, *Phys. Scr.* **T22**, 282 (1988).
- [42] H. Grothe and C. Iselin, CERN Report No. SL 90-13, 1990 (unpublished).
- [43] A. Simonsson, Ph.D. thesis, Manne Siegbahn Institute of Physics and The Royal Institute of Technology, Stockholm, Sweden, 1991.
- [44] S. Schröder *et al.*, *Phys. Rev. Lett.* **64**, 2901 (1990).
- [45] A. Sørensen, in *Proceedings of CERN Accelerator School: Second General Accelerator Physics Course*, Åhus, Denmark, 1986, CERN Report No. 87-10, edited by S. Turner (CERN, Geneva, 1987), p. 135.
- [46] H. Danared (private communication).
- [47] See, for example, W. Schottky, *Ann. Phys.* **57**, 541 (1918); J. Borer, P. Bramham, H. G. Herward, K. Hübner, W. Schnell, and L. Theorndahl (unpublished); H. G. Herward and W. Schnell, in CERN Report No. 77-13, 1977 (unpublished).
- [48] V. V. Avilov and I. Hofmann, *Phys. Rev. E* **47**, 2019 (1993).
- [49] See, for example, S. Chattopadhyay, *Some Fundamental Aspects of Fluctuations and Coherence in Charged-Particle Beams in Storage Rings*, CERN Report No. 84-11 (CERN, Geneva, 1984); D. Habs *et al.*, *Nucl. Instrum. Methods Phys. Res. Sect. B* **43**, 390 (1989); S. Cocher and I. Hofmann, *Part. Accel.* **34**, 189 (1990); D. V. Pestrikov, in *Proceedings of the Workshop on Electron Cooling and New Cooling Techniques* (Ref. [30]), p. 165.
- [50] F. Caspers, in [4].
- [51] W. F. Van Gunsteren and H. J. C. Berendsen, *Groningen Molecular Simulation (GROMOS) Library Manual* (Biomos, Nijenborgh, AG Groningen, The Netherlands, 1987); J. Åqvist, W. F. Van Gunsteren, M. Leijonmarck, and O. Tapia, *J. Mol. Biol.* **183**, 461 (1985).
- [52] J. P. Schiffer and J. S. Hangst, *Z. Phys. A* **341**, 107 (1991).
- [53] R. W. Hasse, *Phys. Rev. A* **46**, 5189 (1992).